Validation of a Two-Phase CFD Model for Autogenous Pressurization and Expulsion

Steven Soriano*
HX5 and NASA Glenn Research Center, Cleveland, OH 44135, USA

Olga Kartuzova† and Mohammad Kassemi‡
National Center for Space Exploration Research (NCSER), Case Western Reserve University and NASA Glenn Research Center, Cleveland, OH 44135, USA

Daniel Hauser §
NASA Glenn Research Center, Cleveland, OH 44135, USA

This paper presents a two-phase CFD model for tank pressurization and expulsion in a liquid hydrogen cryogenic storage tank. The model uses a Volume-of-Fluid approach combined with the Kinetics-based Schrage equation to capture the phase boundary and the associated interfacial heat, mass, and momentum transfer between the liquid and vapor regions. The CFD model is validated against expulsion data from the NASA K-Site tank experiment. Predicted tank pressures, temperatures, and pressurant requirements are compared with the experimental data to demonstrate the model's accuracy.

I. Nomenclature

E	=	Energy
$\mathbf{g}$	=	Gravity
h	=	Surface curvature
k	=	Thermal conductivity
M	=	Molar mass of fluid
p, P	=	Pressure
R	=	Gas constant
T	=	Temperature
t	=	Time
$\mathbf{v}$	=	Velocity
c_p	=	Heat capacity at constant pressure
m	=	Mass

Greek

α	=	Cell value of volume fraction
ϕ	=	Face value of volume fraction
μ	=	Dynamic viscosity
ρ	=	Density
τ	=	Stress tensor
σ	=	Accommodation coefficient

*Mechanical Engineer, Fluid and Cryogenic Systems Branch.
†Research Assistant Professor, Department of Mechanical & Aerospace Engineering, and AIAA Member.
‡Research Professor, Department of Mechanical & Aerospace Engineering, AIAA Associate Fellow.
§Fluids Engineer, Fluid and Cryogenic Systems Branch.

Subscripts

i	=	Interface or phase
l	=	Liquid
v	=	Vapor

II. Introduction

Cryogenic fluid management (CFM) is essential for the future of space exploration and achieving NASA's mission goals. A primary challenge in this domain is effectively managing volatile cryogenic propellants under low-gravity conditions in space. These conditions pose unique difficulties, such as maintaining stable pressure and preventing unwanted phase changes due to microgravity-induced fluid behavior.

To address these challenges, NASA is focused on developing and refining computational fluid dynamics (CFD) models that accurately simulate heat and mass transfer interactions during condensation and evaporation. These models must be validated against ground-based experimental data to ensure their fidelity and reliability for space applications [1]. Validation against experimental data helps identify model deficiencies and provides opportunities for model improvement.

Previous NASA experiments serve as critical validation data for these CFD models. Notably, the data from pressurization experiments conducted at the NASA Plum Brook K-Site Facility are particularly valuable. These experiments provide comprehensive datasets, including pressure, temperature, and mass measurements under controlled conditions closely mimicking tank operations during missions.

This paper advances the field by developing a two-phase CFD model validated against a liquid hydrogen K-Site tank pressurization and expulsion experiment. The model incorporates the Volume-of-Fluid (VOF) method and the Kinetics-based Schrage equation to accurately capture the phase boundary and interfacial heat, mass, and momentum transfer between the liquid and vapor regions. This work addresses a critical gap in validated computational models for large-scale tank experiments involving cryogenic pressurization and expulsion. By enhancing the accuracy and reliability of CFD models, this research contributes to a better understanding and management of cryogenic propellants in space missions.

The validation process involves comparing the CFD model's predicted tank pressures, temperatures, and pressurant requirements with experimental data. The details of the CFD model, including governing equations, boundary conditions, and numerical implementation, are thoroughly presented. Validation results are analyzed to highlight the model's strengths and identify areas for further improvement.

III. Experimental Setup

A. K-Site Testing Facilities

The experiment used for this validation study was performed at NASA Plum Brook K-Site facility [2]. The K-site experiment tank was a 5.8-ft diameter 6061 aluminum tank mounted inside a 25-foot diameter stainless steel vacuum chamber. The tank had an ellipsoidal shape with an internal volume of 61.7 ft^3. Figures 1a and 1b show the tank and its schematic.

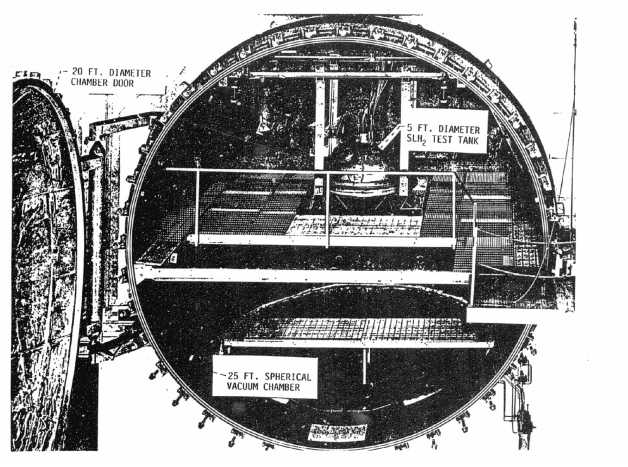

(a) K-Site illustration.

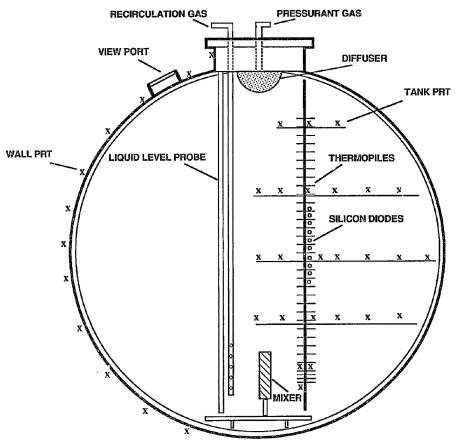

(b) Instrumentation schematic.

Fig. 1 Liquid hydrogen tank tested at K-Site.

This experimental effort aimed to determine the thermodynamic parameters during the ramp pressurization of slush hydrogen (SLH_2) and normal boiling point liquid hydrogen ($NBPH_2$) as part of the National Aero-Space Plane program. This paper focuses on the results with $NBPH_2$. The tests involved pressurizing the tank with gaseous hydrogen from atmospheric pressure to 25, 35, and 50 psia. Following the pressurization, there was a hold phase where the inflow of gaseous hydrogen was reduced to maintain the pressure for a set duration. Finally, gaseous hydrogen flow increased into the tank during the expulsion phase while liquid hydrogen was discharged. The test tank instrumentation, depicted in Figure 1b, included various measuring devices: silicon diodes for monitoring temperatures on the tank walls, internal thermocouples for recording temperatures of both vapor and liquid, pressure transducers, a liquid level probe, and devices to measure the mass flow rate of both the pressurant and propellant streams.

B. Experimental Results

Case 225 from the experimental report [2] was selected for consideration in this report. Case 225 was an $NBPH_2$ pressurization and expulsion test with non-constant inlet gas temperature. Inlet gas temperature increased during the test non-linearly (see Figures 2a and 2b). Figure 3a shows the tank pressure during the complete test, including the pressurization, hold, and expulsion periods. Figure 3b shows the added H_2 mass during the expulsion period, and Figure 3c shows the temperature distribution in the wall and tank near the end of the expulsion period.

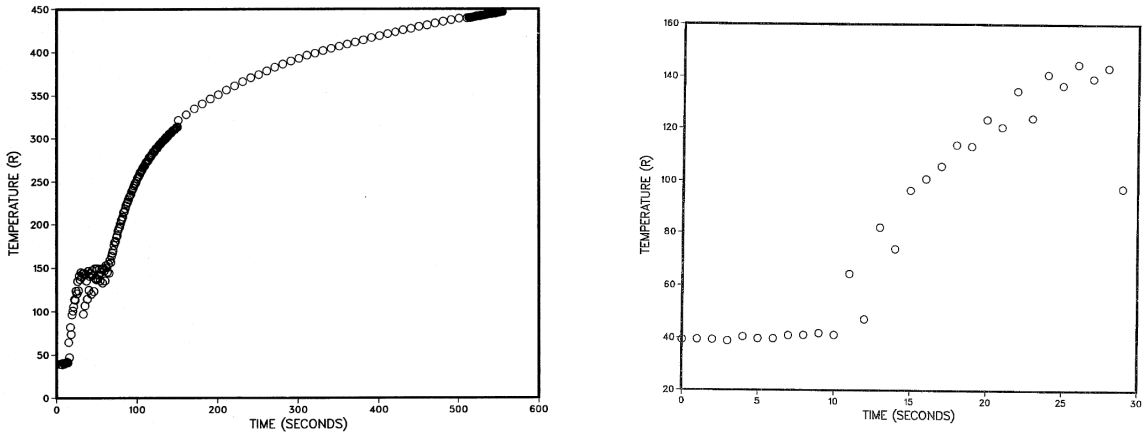

(a) **(b)**

Fig. 2 Inlet gas temperatures: (a) during the complete test, (b) during the pressurization period only.

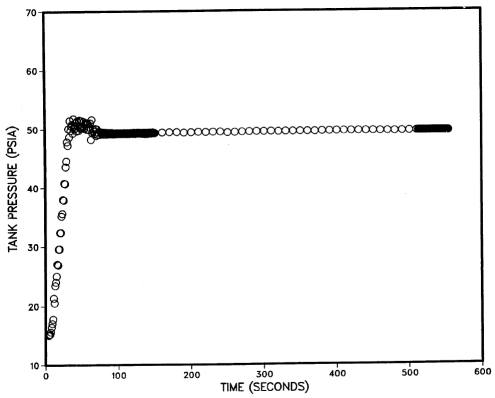

(a) Tank pressure during the experiment.

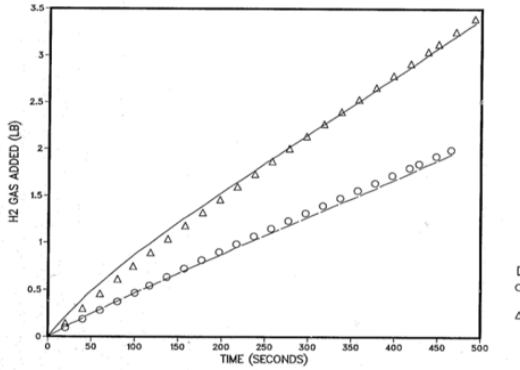

(b) Mass added during the expulsion period.

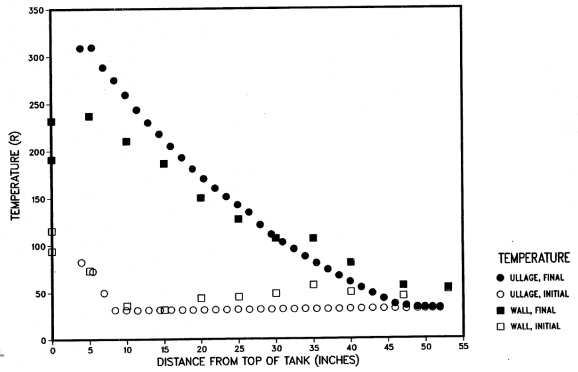

(c) Wall and ullage temperatures near the end of the expulsion period.

Fig. 3 K-site experimental results for Case 225.

It is observed that:

1) There is a slight pressure overshoot before expulsion, indicating a transient system response (Figure 3a).

2) The mass flow rate of gaseous hydrogen during expulsion follows a linear trend, maintaining the tank at the target pressure (Figure 3b).
3) Both ullage and wall temperatures increase during expulsion, showing a slightly curved temperature distribution, indicating non-uniform heating effects (Figure 3c).

IV. Computational Model

A. Governing Equations

Fluid flow and heat transfer in the tank are described in terms of the continuity, Navier-Stokes, and energy equations for both phases:

$$\frac{\partial \rho}{\partial t} + \nabla(\rho \mathbf{v}) = 0, \tag{1}$$

$$\frac{\partial}{\partial t}(\rho \mathbf{v}) + \nabla(\rho \mathbf{v}\mathbf{v}) = -\nabla p + \nabla \left[\mu_{eff}\left(\nabla \mathbf{v} + \nabla v^T\right)\right] + \rho \mathbf{g} + \mathbf{F}_{vol}, \tag{2}$$

$$\frac{\partial}{\partial t}(\rho E) + \nabla(\mathbf{v}(\rho E + p)) = \nabla\left(k_{eff} \nabla T\right) + S_h. \tag{3}$$

The present study treats the liquid phase as incompressible with variable temperature-dependent properties, except for density. The liquid density is allowed to vary linearly with temperature in the body force term of the momentum equation according to the Boussinesq approximation. The vapor is modeled as a compressible ideal gas. In this study, the movement of the interface is captured diffusely using the Volume of Fluid (VOF) method, as published by Hirt and Nichols [3]. Interfacial energy, momentum, and mass balances are applied using source terms in the diffuse interfacial region.

B. VOF Model

In the VOF method, a volume fraction is defined in each cell such that the volume fractions of all the phases sum to unity. In the cell, the change in the interface can be tracked by solving a continuity equation for the volume fraction of the q^{th} phase:

$$\frac{1}{\rho_q}\left[\frac{\partial}{\partial t}\left(\alpha_q \rho_q\right) + \nabla \cdot \left(\alpha_q \rho_q \mathbf{v}_q\right) = S_{\alpha_q}\right], \tag{4}$$

where the volume fraction for the primary phase is determined from:

$$\sum_{q=1}^{n} \alpha_q = 1. \tag{5}$$

In the VOF method, the field variables and properties are defined in terms of the volume fraction, which for a general system can be written as:

$$\rho = \sum_{q=1}^{n} \alpha_q \rho_q, \quad \mu_{eff} = \sum_{q=1}^{n} \alpha_q \mu_{eff_{q'}} \quad k_{eff} = \sum_{q=1}^{n} \alpha_q k_{eff_q}. \tag{6}$$

In this fashion, the continuity, momentum, and energy equations, as described by Eq. (1)-(3), can be solved throughout the domain for the temperatures and velocities in the two phases. In the VOF model, energy (E) and temperature (T) are treated as mass-averaged variables:

$$E = \frac{\sum_{q=1}^{n} \alpha_q \rho_q E_q}{\sum_{q=1}^{n} \alpha_q \rho_q}, \tag{7}$$

where E_q is based on the specific heat of the q^{th} phase and the shared temperature.

Evaporation and condensation at the interface are modeled as a source term in the continuity equation for the volume fraction (Eq. 4), i.e.:

$$S_{\alpha_q} = \dot{\mathbf{m}}_i \cdot \mathbf{A}_i, \tag{8}$$

where $\mathbf{A}_i$ is an interfacial area density vector, and $\dot{\mathbf{m}}_i$ is a mass flux vector, which for near equilibrium conditions can be determined based on the Schrage equation [4]:

$$|\dot{\mathbf{m}}| = \left(\frac{2\sigma}{2-\sigma}\right)\left(\frac{M}{2\pi R}\right)^{1/2}\left(\frac{P_i}{T_i^{1/2}} - \frac{P_v}{T_v^{1/2}}\right). \tag{9}$$

Here σ is the accommodation coefficient (a value of 0.001 was used for the CFD simulations); M is the molar mass of the fluid; R is the universal gas constant; P_i and P_v are, respectively, the interfacial and vapor pressures (it was assumed that $P_i \cong P_{sat}$); T_i and T_v are, respectively, the interfacial and vapor temperatures (it was assumed that $T_i = T_v \cong T_{sat}$ at the interface). Finally, $\mathbf{A}_i$ is defined as:

$$\mathbf{A}_i = |\nabla \alpha|, \tag{10}$$

where α is the volume fraction of the primary phase.

In the present implementation, the surface tension forces at the interface are modeled via the Continuum Surface Force (CSF) model of Brackbill et al. [5]. In this model, the surface tension forces at the interface are transformed into a volume force ($\mathbf{F}_{vol}$), which is added as a source to the momentum equation:

$$\mathbf{F}_{\text{vol}} = \sum_{\text{pairs } ij, i<j} \sigma_{ij} \frac{\alpha_i \rho_i h_i \nabla \alpha_j + \alpha_j \rho_j h_j \nabla \alpha_i}{\frac{1}{2}\left(\rho_i + \rho_j\right)}, \tag{11}$$

where h_i is the surface curvature calculated from the local gradients in the surface normal at the interface:

$$h_i = \nabla \cdot \hat{\mathbf{n}}. \tag{12}$$

V. Numerical Implementation

In CFD simulations, just like in the physical experiment, the process starts by pressurizing the tank with gaseous hydrogen. This is achieved using a diffuser at the top of the tank, as shown in Figure 4. After the tank's pressure hits the target pressure, the gas inflow is significantly reduced. This step, known as the "hold" period in experiments, keeps the tank pressure stable. Once this hold period ends, expulsion begins, with liquid hydrogen exiting the tank, and the inflow of pressurant gas is again increased to keep the tank pressure constant at a target value. Test case 225 was selected for model validation.

All simulations were conducted using ANSYS Fluent 2024 R1[6]. A custom in-house user-defined function (UDF) was employed to implement the VOF and mass transfer model described in Section IV.B.

A. Tank Geometry

A 1.79 m diameter K-Site Tank was used for model validation. Figure 4 shows a schematic of the tank. Gas is assumed to enter the tank uniformly and perpendicular to the diffuser. In the experiment, the incoming gas passed through a screen before entering the tank. The outlet is directly under the gas inlet.

Table 1 K-Site test parameters.

Case #	Ullage Volume, %	Initial Pressure, psia	Ramp Pressure, psia	Expulsion Pressure, psia	Ramp Time, s	Hold Time, s	Expulsion Time, s
225	8.4	15	51.5	48.9	30	30	500

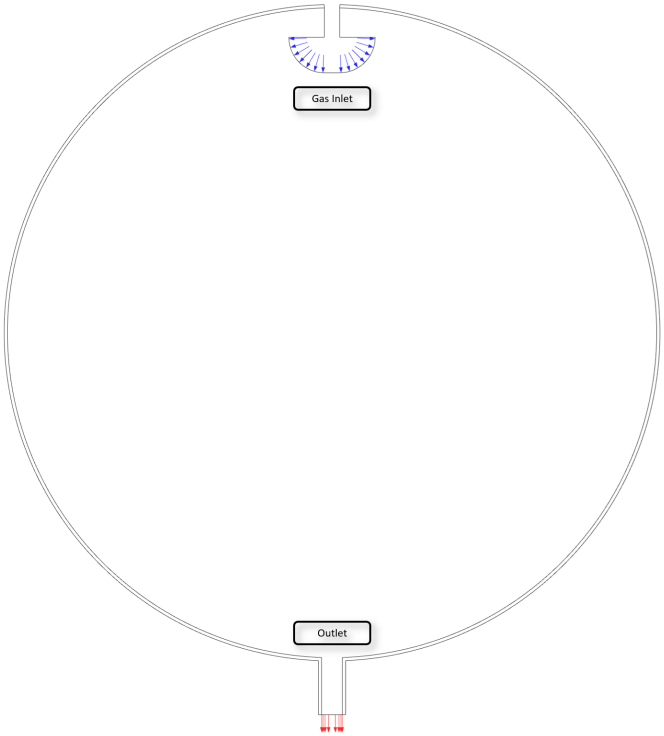

Fig. 4 Tank geometry used for CFD.

B. Initial Conditions

To begin modeling the pressurization period, the initial tank pressure was set to the experimental value for case 225, and the initial ullage volume was set to the corresponding experimental value as reported in Table 1. Liquid and vapor temperatures were set to saturation values at the initial tank pressure. A 2D axisymmetric model was employed to simplify the computational domain. A laminar model was used to model the flow within the tank.

C. Boundary Conditions

The CFD model included conjugate heat transfer through the aluminum wall. Non-slip boundary conditions are applied on the inside of the tank wall, and the contact angle between the liquid and tank wall is set to 0 degrees. The outlet is modeled as a wall during the pressurization and hold periods. The outlet is then prescribed a mass outlet boundary condition during expulsion. Gaseous hydrogen is injected at the gas inlet, as shown in Figure 4, and the inlet gas temperature is matched to the experimental values shown in Figures 2a and 2b. Figure 2a shows the inlet gas temperatures during the complete test, including pressurization, hold, and expulsion, and Figure 2b shows the inlet gas temperatures for the pressurization period only.

Experimental transient inlet mass flow rate data was not reported for this case. Instead, the mass added at the end of pressurization and during expulsion was provided. To estimate the inlet mass flow rate, we conducted numerous simulations by dividing the added mass at the end of pressurization by the pressurization duration, creating a pseudo-inlet mass flow rate. These simulations indicated that the resulting added mass was insufficient to achieve the target pressure within the reported time frame. Due to uncertainties in the experimental data during pressurization and discrepancies shown by CFD simulations, a pressure boundary condition was used to implement a pressure ramp leading to the

target pressure for expulsion. Inlet gas temperatures for CFD were kept consistent with the experiment, and a pressure controller was used to regulate the pressure during the expulsion. The outlet mass flow rate matched the experimental value during expulsion (0.217 kg/s).

D. Material Properties

The material properties of liquid hydrogen and its vapor were sourced as properties of parahydrogen from the NIST REFPROP database. For each case, constant saturation properties at the initial tank pressure were used, except for specific heat, thermal conductivity, and vapor viscosity, which varied with temperature.

E. Computational Mesh

The computational mesh used for the simulations was an unstructured mesh of 21,711 cells, as depicted in Figure 5. Mesh refinement was included near the tank walls.

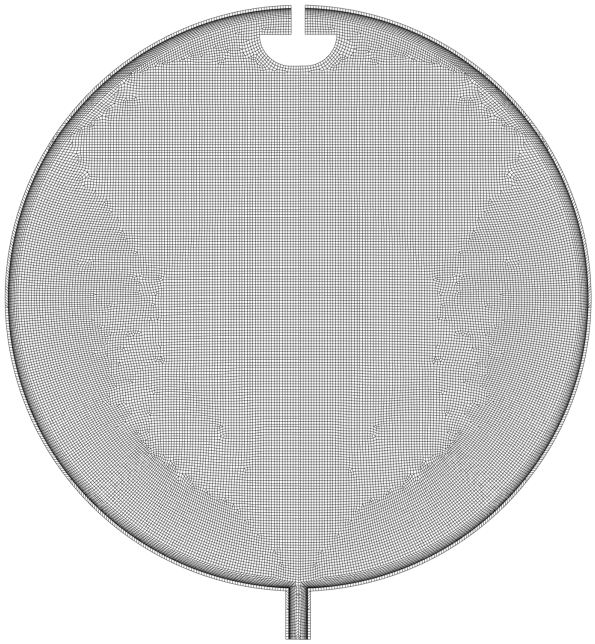

Fig. 5 Computational mesh.

VI. Results & Discussion

CFD results were compared with experimental results. Figure 6 displays CFD and experimental tank pressure evolutions throughout the test stages. Additionally, Figure 7 shows the CFD-predicted phase change rate in the tank, for which no experimental data is available. As outlined in Section V.C, a pressure boundary condition was implemented for the pressurization and hold phases of the simulation, addressing uncertainties in the experimental data and discrepancies observed in CFD outcomes. A controller was used to regulate the pressure in the tank during the expulsion process. Figure 6 illustrates a slight decrease in pressure at the beginning of the expulsion, which stabilizes at the target pressure (48.9 psi) for the remainder of the simulation. This initial dip in pressure occurs as the liquid is expelled from the tank, expanding the vapor volume. During this phase, the influx of pressurant gas is insufficient to immediately counterbalance the pressure drop, further influenced by vapor condensation at the interface. This is a preliminary result, and the controller will be adjusted to eliminate the pressure drop. Figure 7 shows condensation occurring during the pressurization and holds where the vapor pressure at the interface is increasing and overcoming the saturation point. At the start of expulsion, there is an interplay between evaporation and condensation; throughout the expulsion, condensation is prevalent. This interplay between evaporation and condensation is attributed to vapor pressure increasing relative to the saturation point and hotter inlet gas reaching the interface, causing liquid at the interface to evaporate.

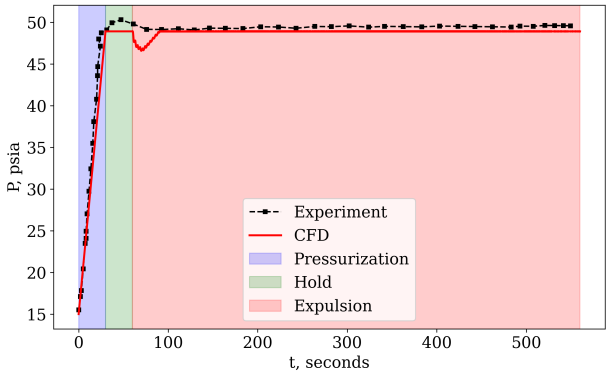

Fig. 6 Tank pressure during stages of the test: Experiment versus CFD.

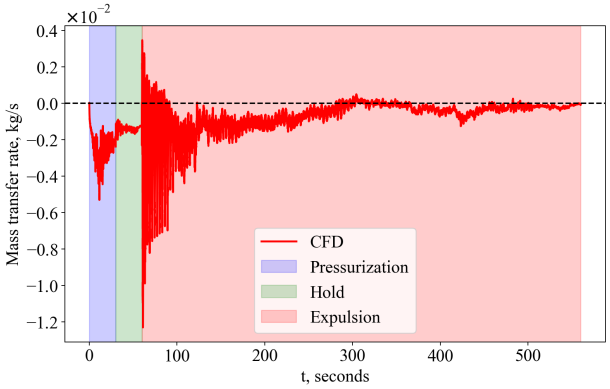

Fig. 7 Predicted phase change rate in the tank during stages of the test.

Figure 8 displays the added pressurant gas during expulsion, comparing CFD results with experimental data. The predicted CFD added pressurant at the end of the expulsion matches experimental values within 1%. Although adjustments will be made to the controller to address the observed pressure drop, these changes are not expected to alter this curve significantly.

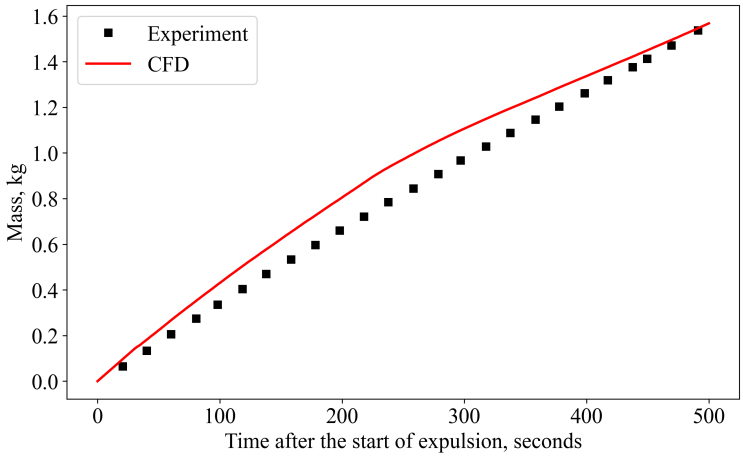

Fig. 8 Added pressure gas during the expulsion: Experiment vs CFD.

In the experiment, thermocouples measured the internal temperature distribution within the tank and along the tank wall. These thermocouples were placed off-center from the tank's center line (Figure 1b). Temperature monitors in the CFD model were positioned at the same locations as in the experiment. Figure 9 shows the temperature distribution in the tank and along the tank wall for both the CFD results and the experiment near the end of expulsion. The CFD temperature distribution in the tank follows the experimental trend but slightly overpredicts the temperature values. Similarly, the CFD wall temperatures follow the experimental trend but slightly overpredict the values. This slight overprediction might be due to using a laminar model for the flow field. The laminar model may not account for turbulent mixing, which could result in higher vapor temperatures. A turbulent case will also be presented in the final paper to compare results.

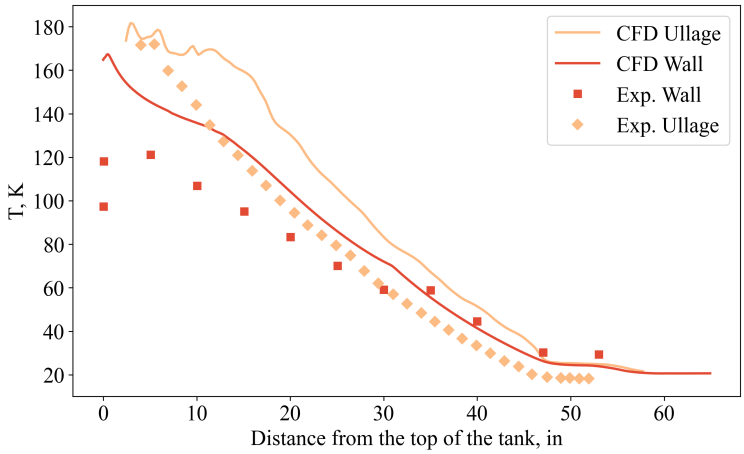

Fig. 9 Wall and ullage temperature distribution in the tank near the end of the expulsion (t=493s) compared to experimental values.

Figure 10 shows the temperature evolution during the expulsion at a specific temperature monitor, TP 34, located in the upper ullage. The CFD results at this location are plotted alongside the experimental temperature data. It can be observed that the CFD temperature closely aligns with both the magnitude and trend of the experimental values.

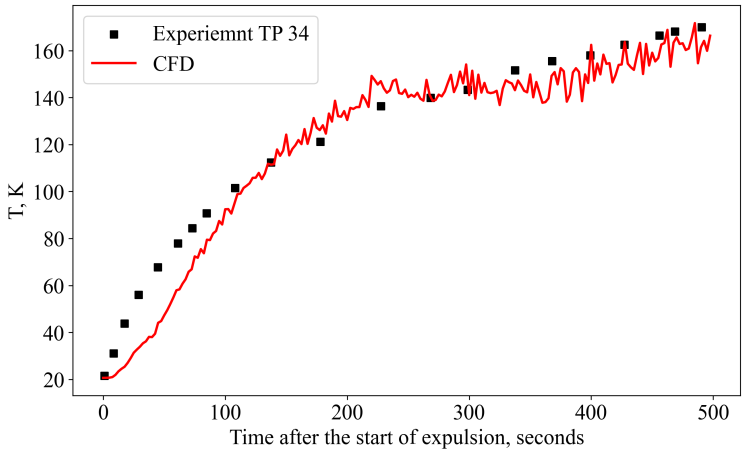

Fig. 10 Wall and ullage temperature distribution in the tank near the end of the expulsion (t=493s) compared to experimental values.

Further discussion will be provided in the final paper and results using a turbulent model will be presented.

VII. Conclusion

The conclusion will be provided in the final paper.

Acknowledgments

The authors thank the Modeling Portfolio Project within the STMD CFM Project Office for funding this work.

References

[1] Kartuzova, O. V., Kassemi, M., and Hauser, D. M., "Validation of a Two-Phase CFD Model for Predicting Propellant Tank Pressurization and Pressure Collapse in The Ground-Based K-Site Hydrogen Slosh Experiment," *AIAA SCITECH 2024 Forum*,

2024, p. 0547.

[2] Whalen, M. V., Hardy, T. L., Tomsik, T. M., Mahoney, N. B., and DeWitt, R. L., "Comparison of Pressurized Expulsion of Slush Hydrogen and Normal Boiling Point Liquid Hydrogen Using Hydrogen Pressurant Gas," Tech. rep., National Aerospace Plane (NASP) Technical Memorandum, 1991.

[3] Hirt, C. W., and Nichols, B. D., "Volume of fluid (VOF) method for the dynamics of free boundaries," *Journal of computational physics*, Vol. 39, No. 1, 1981, pp. 201–225.

[4] Schrage, R. W., *A theoretical study of interphase mass transfer*, Columbia University Press, 1953.

[5] Brackbill, J. U., Kothe, D. B., and Zemach, C., "A continuum method for modeling surface tension," *Journal of computational physics*, Vol. 100, No. 2, 1992, pp. 335–354.

[6] *ANSYS Fluent User's Guide*, ANSYS, Inc., release 24.1 ed., 2023.